

Near-Infrared Spectroscopy of Photodissociation Regions: The Orion Bar and Orion S

K. L. Luhman¹, C. W. Engelbracht¹, and M. L. Luhman^{2,3}

kluhman@as.arizona.edu, chad@as.arizona.edu, luhman@irfp1.nrl.navy.mil

ABSTRACT

We have obtained moderate-resolution ($R \sim 3000$) spectra of the Orion bar and Orion S regions at J ($1.25 \mu\text{m}$), H ($1.64 \mu\text{m}$), and K ($2.2 \mu\text{m}$). Towards the bar, the observations reveal a large number of H_2 emission lines that, when compared to model predictions of Draine & Bertoldi (1996), are indicative of a high-density photodissociation region (PDR) ($n_{\text{H}} = 10^6 \text{ cm}^{-3}$, $\chi = 10^5$, $T_0 = 1000 \text{ K}$) rather than shocked material. Behind the bar into the molecular cloud, the H_2 spectrum again matches well with that predicted for a dense PDR ($n_{\text{H}} = 10^6 \text{ cm}^{-3}$) but with a lower temperature ($T_0 = 500 \text{ K}$) and UV field strength ($\chi = 10^4$). The H_2 spectrum and stratification of near-IR emission lines (O I, H I, [Fe II], [Fe III], H_2) near Orion S imply the presence of a dense PDR with an inclined geometry in this region as well ($n_{\text{H}} = 10^6 \text{ cm}^{-3}$, $\chi = 10^5$, $T_0 = 1500 \text{ K}$). The extinction measurements towards the bar ($A_{\text{K}} \sim 2.6$) and Orion S ($A_{\text{K}} \sim 2.1$) H_2 emission regions are much larger than expected from either face-on ($A_{\text{K}} \sim 0.1$) or edge-on ($A_{\text{K}} \sim 1$) homogeneous PDRs, indicating that clumps may significantly affect the structure of the PDRs.

In addition, we have observed the strongest ~ 30 near-IR He I emission lines, many of which have not been detected previously. There is good agreement between most observed and theoretical He I line ratios, while a few transitions with upper levels of $n^3\text{P}$ (particularly $4^3\text{P} - 3^3\text{S}$ $1.2531 \mu\text{m}$) are enhanced over strengths expected from collisional excitation. This effect is possibly due to opacity in the UV series $n^3\text{P} - 2^3\text{S}$. We also detect several near-IR [Fe II] and [Fe III] transitions with line ratios indicative of low densities ($n_{\text{e}} \sim 10^3\text{-}10^4 \text{ cm}^{-3}$), whereas recent observations of optical [Fe II] emission imply the presence of high-density gas ($n_{\text{e}} \sim 10^6 \text{ cm}^{-3}$). These results are

¹Steward Observatory, University of Arizona, Tucson, AZ 85721.

²Naval Research Laboratory, Remote Sensing Division, Code 7217, Washington, DC 20375

³NRC-NRL Research Associate

consistent with a model in which high-density, partially-ionized gas is the source of the iron transitions observed in the optical while low-density, fully-ionized material is responsible for the near-IR emission lines.

Subject headings: infrared: ISM: lines and bands — ISM: individual (Orion Nebula) — ISM: molecules — ISM: structure

1. Introduction

The Orion Nebula is an excellent laboratory for the study of various phenomena occurring in the interstellar medium. Within this region, the Orion bright bar has proven especially useful in understanding the detailed structure of photodissociation regions (PDRs), which have become a subject of intensive theoretical modeling in recent years (Tielens & Hollenbach 1985; Burton, Hollenbach, & Tielens 1990; Sternberg & Dalgarno 1995; Draine & Bertoldi 1996, hereafter DB96) with particular emphasis on the ultraviolet (UV) excitation of H₂ and the subsequent fluorescent infrared (IR) emission-line spectra (Black & van Dishoeck 1987; Sternberg & Dalgarno 1989). As a relatively nearby (~ 450 pc) and apparently edge-on PDR, the chemical and thermal stratification within the Orion bar has been well-resolved and compared extensively to model predictions (Tielens et al. 1993; Omodaka et al. 1994; Tauber et al. 1994; Hogerheijde, Jansen, & van Dishoeck 1995; Jansen et al. 1995; Usuda et al. 1996; van der Werf et al. 1996).

Near-IR spectroscopy of PDR emission features, particularly H₂ 1-0 S(1) and 2-1 S(1), has been performed towards the Orion bar (Hayashi et al. 1985; Burton et al. 1990; Sellgren, Tokunaga, & Nakada 1990; Marconi et al. 1997), but with recent advances in near-IR spectrometers we can now reveal the entire IR spectrum of the Orion PDRs in much greater detail than previously possible. For instance, in H- and K-band spectra of the planetary nebula Hubble 12, which is a source of pure H₂ fluorescence arising in low-density gas ($n_{\text{H}} \leq 10^4\text{-}10^5 \text{ cm}^{-3}$), Luhman & Rieke (1996) found excellent agreement between the observed line ratios of more than 30 H₂ transitions and the values predicted by theoretical models (Black & van Dishoeck 1987). In addition to H₂, these spectra of Hubble 12 included many transitions in He I, [Fe II], and [Fe III], providing tests of the model near-IR spectra of these species. To test the PDR model spectra under the physical conditions (temperature, UV field strength, density) present in Orion, we have obtained moderate-resolution ($R \sim 3000$) J-, H-, and K-band long-slit spectra of the Orion bar and a bright emission region $\sim 40''$ southwest of the Trapezium stars, commonly known as Orion S (Ziurys et al. 1981). These observations provide conclusive evidence for the PDR

origin (rather than shocks) of the H₂ emission in each of these regions and demonstrate significant departures in the observed chemical structure from that predicted by models of homogeneous PDRs.

2. Observations

On 1995 December 8-10, we performed spectroscopy at J (1.25 μm), H (1.64 μm), and K (2.2 μm) towards the Orion bright bar and Orion S region using the near-IR long-slit spectrometer FSpec (Williams et al. 1993) at the Steward 1.55 m Bigelow Reflector. Using a 128 \times 128 IR camera as an off-the-slit guider, we obtained H-band images at each slit position as a check of the exact coordinates of our apertures. For Orion S, the 3".5 \times 130" slit (= 2 \times 75 pixels) was aligned east-west and centered at $\alpha = 5^{\text{h}}35^{\text{m}}16^{\text{s}}.8$, $\delta = -5^{\circ}23'59''$ (2000). In the second set of observations, the slit was perpendicular to the bar (PA = 135 $^{\circ}$) and centered at $\alpha = 5^{\text{h}}35^{\text{m}}20^{\text{s}}.3$, $\delta = -5^{\circ}25'06''$ (2000). One grating setting in J, H, and K covered 0.03, 0.1, and 0.1 μm with a two-pixel resolution of $\lambda/\Delta\lambda = 3200$, 2400, and 3200, respectively, providing full coverage of these bands with a total of 16 grating settings. For each grating setting, we obtained four exposures of 60 s on the source in addition to four exposures 5' to the west to provide a measurement of the sky background. We then observed a telluric standard star by stepping it through six positions along the slit. Due to poor weather conditions while obtaining data longward of 2.3 μm , we repeated the K-band observations at the 2.3 m Bok Reflector on Kitt Peak during 1996 October 28 and 29. The slit was 2".4 \times 90" (= 2 \times 75 pixels) at this telescope, but otherwise these observations were identical to the previous ones.

IRAF routines and customized scripts within this environment were used to reduce the data. After dark subtraction and flat-fielding, off-source images were subtracted from on-source data to remove sky emission. For a given grating setting, four sky-subtracted images were combined, during which most transient bad pixels (e.g., cosmic rays) were rejected. Each combined image was then divided by the spectrum of the standard star to correct for telluric absorption (see § 3.2). The resulting image at each grating setting, consisting of 256 pixels along the dispersion axis and 75 pixels in the spatial direction, was wavelength calibrated using OH airglow lines and Ne-Kr lamp spectra. To correct for slight guiding errors, we used the stars falling in the slit and the spatial variation of the hydrogen lines to align images from consecutive grating settings, which were then combined into one image spanning J (1.25-1.34 μm), H (1.45-1.75 μm), and K (2.0-2.45 μm). The spatial offsets were always less than 2 pixels. Since each grating setting overlapped by 50% with its neighboring spectrum (e.g., 2.04-2.14 μm , 2.09-2.19 μm , etc.), virtually every emission line

appeared in two grating settings. Consequently, we were able to achieve accurate relative calibration ($< 5\%$) across each band. The telluric standard at H was a G star (HR 2007), the stellar spectral slope and absorption features of which were removed from the Orion data by applying the solar spectrum, as discussed by Maiolino, Rieke, & Rieke (1996). The Orion data at J and K were multiplied by a blackbody of $T = 9900$ K to correct for the slope introduced by the A-star telluric standard used in these bands (HR 1489 with stellar Pa β and Br γ absorption removed artificially).

3. Results

3.1. Extraction of Spectra and Flux Calibration

To select apertures for the extraction of spectra, we examined the spatial distribution of the major emission lines of each species in the bar and Orion S, as illustrated in Figures 1 and 2. Since the slit was 2 pixels wide and the data were binned by 2 pixels along the slit, each point in these profiles represents a 2×2 pixel region, where one pixel is $1.75''$ and $1.2''$ for the 1.55 m and 2.3 m data, respectively. Three $20''$ apertures shown in Figure 1 sample three distinct regions of emission in the bar: beyond the bar towards the molecular cloud (Bar1), on the peak of H $_2$ emission (Bar2), and in front of the bar towards the H II region (Bar3). With the large spatial overlap of the various emission features in Orion S, we extracted one $38''$ aperture which included the bulk of the emission in each species. Due to the poor quality of the 1.55 m data beyond $2.2 \mu\text{m}$ (see § 2), the K-band spectra from the 2.3 m telescope were used to analyze emission in [Fe III] towards Bar3 and Orion S and H $_2$ towards Bar1, Bar2, and Orion S. Since the H $_2$ emission towards the H II region in Bar3 probably originates from many regions along the line of sight rather than a well-defined zone of the PDR, we do not model the H $_2$ in Bar3. The J-, H-, and short K-band ($2.0\text{-}2.2 \mu\text{m}$) data were used to examine the line ratios of He I and [Fe II] in Bar3 and Orion S. The spectra for Orion S are shown in Figures 3, 4, and 5. The spectra for Bar1, Bar2, and Bar3 are not shown since the combined data appear qualitatively similar to those of Orion S.

Due to guiding errors in observing a standard star with a long-slit spectrometer, flux calibration between J, H, and K is relatively uncertain ($\pm 20\text{-}30\%$). To facilitate comparison of line strengths across the bands, we calibrated the J- and H-band spectra such that the strengths of the hydrogen recombination lines relative to Br γ matched the case B predictions of Storey & Hummer (1995) for a plasma with $n_e = 10^2 \text{ cm}^{-3}$ and $T_e = 10^4$ K. These predicted line ratios do not depend substantially on density and temperature for the range of values likely in Orion. This procedure should also correct the differential extinction (as measured towards the ionized gas) between the bands. The Br γ fluxes are 4.4 ± 0.5

and $(15 \pm 2) \times 10^{-12}$ erg s⁻¹ cm⁻² towards the Bar3 ($3''.5 \times 20''$) and Orion S ($3''.5 \times 38''$) apertures extracted from the 1.5 m data, respectively. In the Bar1 and Bar2 ($2''.4 \times 20''$) and Orion S ($2''.4 \times 38''$) apertures extracted from the 2.3 m data, the fluxes of 1-0 S(1) are 0.8 ± 0.15 , 2.0 ± 0.4 , and $(5.6 \pm 1) \times 10^{-13}$ erg s⁻¹ cm⁻², respectively. In Figures 1 and 2, the maximum values of Br γ for the bar and Orion S are 1.04 and 1.61×10^{-12} erg s⁻¹ cm⁻² in $3''.5 \times 3''.5$, corresponding to 3.61 and 5.59×10^{-3} erg s⁻¹ cm⁻² sr⁻¹. Relative to these Br γ measurements, the peak respective values of H₂ 1-0 S(1), O I 1.3169 μ m, [Fe II] 1.6440 μ m, and [Fe III] 2.2183 μ m are 0.10, 0.12, 0.15, and 0.024 for the bar and 0.13, 0.19, 0.13, and 0.017 for Orion S.

3.2. Telluric Correction in Near-IR Emission Line Spectra

As discussed in § 2, we attempted to remove telluric absorption in the Orion spectra through division by a standard stellar spectrum. This procedure works well with spectra of continuum objects (e.g., stars) but can be problematic with emission-line spectra. At moderate spectral resolution (100 km s⁻¹) we cannot observe the true atmospheric transmission, which is dominated by narrow (10 km s⁻¹), optically thick absorption features. As a result, the combination of these telluric absorption features and intrinsically narrow (5-20 km s⁻¹) astronomical emission lines produces systematic errors in the measured line fluxes of the latter. For instance, an emission line passing through a telluric feature is suppressed (or even totally blocked) and cannot be recovered since the narrow telluric line is smoothed to moderate resolution. On the other hand, if an emission line is fully transmitted but falls near a deep absorption feature, division by the telluric standard spectrum, in which the absorption feature is now smoothed to overlap with the emission line, can artificially boost the emission-line flux.

We have modeled these effects with the ultra-high resolution ($R > 10^5$) atmospheric transmission spectrum obtained by Livingston & Wallace (1991). For the H₂ emission region in the bar, we assumed $V_{\text{LSR}} = 10\text{-}11$ km s⁻¹ as measured for CO towards the bar by Omodaka et al. (1994) and van der Werf et al. (1996) and an intrinsic thermal line width of FWHM = 5 km s⁻¹ (T = 1500 K). Since the Orion S region has not been studied extensively, the representative velocity and line width for this region is uncertain. CO measurements indicate two lobes of $V_{\text{LSR}} = 0\text{-}3$ and $11\text{-}16$ km s⁻¹ (Schmid-Burgk et al. 1990; Wilson & Mauersberger 1991) which may trace shocked material, while a velocity intermediate between these and similar to that in the bar would be expected if PDR emission is dominant. Consequently, the velocity of the material in the bar (~ 10 km s⁻¹) should be roughly appropriate for the Orion S region. We then model line

widths characteristic of H₂ from both a PDR (5 km s⁻¹) and shocked region (20 km s⁻¹). Finally, to model the telluric correction for H I and He I lines arising in the ionized gas we adopt $V_{\text{LSR}} \sim -1$ km s⁻¹ (O’Dell 1994) and a line width of FWHM = 20 km s⁻¹ (typical for ionized gas in H II regions).

Figure 6 shows the results of our modeling for all H₂ transitions and the prominent H I and He I lines appearing in our moderate-resolution K-band spectra of the bar and Orion S for the range of velocities observable during a year. As expected, comparison of the two models for the H₂ transitions indicates that narrow emission lines are affected more dramatically. Lines falling within the telluric CO₂ bands centered at 2.01 and 2.06 μm and in the water absorption beyond 2.35 μm are most susceptible to systematic errors in measured line fluxes. In fact, 2-1 S(4) 2.0041 μm and He 2.0587 μm (see § 4.2) deviate so rapidly with velocity that they cannot be measured reliably. On the other hand, lines falling in other regions of the K-band, particularly Br γ , 1-0 S(1), and 2-1 S(1), are unaffected at the 2% level over the range of velocities in question. Although it falls within the water bands, 1-0 Q(4) 2.4375 μm may avoid contamination as long as it is redshifted away from a broad, opaque atmospheric absorption feature to the immediate blueward side. The H₂ transition 1-0 S(2) 2.0338 μm is also relatively free of contamination since it falls between the CO₂ bands. Since these two transitions, 1-0 Q(4) and 1-0 S(2), share the same upper level and cover a large spectral baseline, they can prove useful as an extinction diagnostic (§ 4.1.1). The other Q-branch transitions show much larger deviations in measured line strengths, as do 2-1 S(0) and 3-2 S(1). Fortunately, at the time of our observations the error factors were relatively small (< 25%) and do not change significantly with the observed velocity (V_{obs}) or line width (FWHM). We find that the prominent H I, He I, and [Fe II] lines in the J and H windows are relatively unaffected by problems with telluric correction since the regions near these lines lack dense groupings of opaque telluric lines. However, there are many relatively isolated, narrow (~ 20 km s⁻¹) absorption lines which are opaque and can suppress astronomical emission lines which happen to have the appropriate velocity shift, although this is not a problem for the Orion data presented here.

4. Discussion

4.1. Molecular Hydrogen Lines

4.1.1. Extinction Towards the H₂ Emission Regions

We have detected emission in 17 transitions of H₂ in our K-band spectra of the bar and Orion S. The H₂ line ratios measured in the Bar1, Bar2, and Orion S apertures (see

§ 3.1) are given relative to 1-0 S(1) in Table 1. The uncertainties in the line ratios reflect measurement errors in individual lines in addition to uncertainties in the relative flux calibration among various grating settings (§ 2). As discussed in § 3.2 and illustrated in Figure 6, imperfect telluric correction produces large systematic errors in measurements of several transitions. Given approximate values of the velocities and line widths of the emitting regions and the dates of observations, we have divided the H₂ fluxes measured at 2.0656, 2.3556, 2.3865, 2.4066, 2.4134, and 2.4237 μm by the estimated correction factors of 1.3, 1.1, 1.1, 1.2, 1.1, and 1.15 (see Figure 6), respectively. Since emission in 1-0 Q(5) 2.4547 μm is contaminated substantially by atmospheric absorption, we do not attempt to correct this line strength and omit it from our discussion.

For comparison to H₂ spectra predicted by PDR models (see § 4.1.2), we must deredden the observed line ratios. In our K-band data, there are three pairs of transitions, 1-0 Q(2)/1-0 S(0), 1-0 Q(3)/1-0 S(1), and 1-0 Q(4)/1-0 S(2), with the same upper levels which can be used to estimate the extinction. Before using the first of these ratios, we have deblended 1-0 S(0) from an unidentified emission line which appears in the red wing of this H₂ line at $\sim 2.2245 \mu\text{m}$. This unidentified feature appears to arise from an atomic species (see § 4.4) and contaminates the 1-0 S(0) line towards only the Orion S aperture, which encompasses both molecular and ionized emission regions. Using a form of the IR interstellar extinction law where $A_\lambda = A_K(\lambda/2.2 \mu\text{m})^{-1.75}$, which is equivalent to that of Rieke & Lebofsky (1985), we derived reddenings of $A_K = 1.5 \pm 0.7$, 2.5 ± 0.3 , and 1.5 ± 0.6 for Orion S and $A_K = 3.3 \pm 1$, 2.7 ± 0.4 , and 1.3 ± 1.7 for Bar2 from 1-0 Q(2)/1-0 S(0), 1-0 Q(3)/1-0 S(1), and 1-0 Q(4)/1-0 S(2), respectively. For the Bar1 position, we arrived at $A_K = 2.8 \pm 1.3$ and 2.1 ± 0.6 from 1-0 Q(2)/1-0 S(0) and 1-0 Q(3)/1-0 S(1) [1-0 Q(4) was not detected]. The weighted averages are $A_K = 2.3 \pm 0.8$, 2.6 ± 0.7 , and 2.1 ± 0.5 for Bar1, Bar2, and Orion S.

After applying the atmospheric correction factors to the observed data, the extinction values were used to deredden the H₂ line ratios, which are presented in Table 1 and compared to PDR model predictions in § 4.1.2. The origin of these large reddenings towards the H₂ emission regions is discussed in § 4.1.4. We note that previous observations have also hinted at unexpectedly large extinction. Sellgren et al. (1990) observed Q-branch emission ($\sim 2.4 \mu\text{m}$) which was very strong relative to 1-0 S(1), although this effect was attributed at the time to differing spatial scales in the separate observations of the Q-branch and 1-0 S(1) emission.

4.1.2. Comparison of the H_2 Spectra to PDR Model Predictions

We now compare the “corrected” H_2 line ratios in Table 1 to those predicted by recent PDR models of DB96. In modeling the bar and Orion S, we considered a range of values for the density ($n_H = 10^2$ - 10^6 cm^{-3}), temperature ($T_0 = 300$ - 2000 K), and UV field strength ($\chi = 10^2$ - 10^6). Note that the definitions of these parameters, given in DB96, are not identical among available PDR models. By dereddening the data in Table 1, we have corrected for the effect of PDR inclination on the observed line ratios and we need only consider face-on geometries. After comparing the various model spectra to the corrected line ratios for the Bar2 aperture, which includes the peak of the H_2 emission, we find an excellent fit with $n_H = 10^6$ cm^{-3} , $\chi = 10^5$, and $T_0 = 1000$ K. As shown in Table 1, nearly all line ratios match the data within the observational uncertainties. No other combination of parameters produced a comparable fit. These values for the density, temperature, and UV field strength agree well with previous estimates towards the dense component of the PDR (e.g., van der Werf et al. 1996), which apparently dominates the H_2 emission (see § 4.1.3). For the Bar1 aperture, which includes fainter emission beyond the bar, we find a very good fit with $n_H = 10^6$ cm^{-3} , $\chi = 10^4$, and $T_0 = 500$ K. Marginal fits were produced with ($n_H = 10^5$ cm^{-3} , $\chi = 10^4$, $T_0 = 1000$ K), ($n_H = 10^6$ cm^{-3} , $\chi = 10^4$, $T_0 = 300$ K), and ($n_H = 10^6$ cm^{-3} , $\chi = 10^5$, $T_0 = 500, 1000$ K). Consequently, the H_2 emission in the Bar1 aperture appears to originate in a dense PDR, just as in the Bar2 aperture. Towards Bar1 the temperature is lower and the UV field is attenuated, which is consistent with the location of this emission region behind the bar and deeper into the molecular cloud. The data for Orion S is matched well with two sets of models which produce nearly identical line ratios, ($n_H = 10^5$ cm^{-3} , $\chi = 10^4$, $T_0 = 1500$ K) and ($n_H = 10^6$ cm^{-3} , $\chi = 10^5$, $T_0 = 1500$ K). Since the Orion S region is closer, at least in projection, to the ionizing stars than the bar, the model with $\chi = 10^5$ is probably more appropriate and is shown in Table 1. Therefore, only the temperature differs between the best models for the Bar2 ($T_0 = 1000$ K) and Orion S ($T_0 = 1500$ K) positions. As seen in Table 1, the line ratios, particularly $F[2-1 S(1)]/F[1-0 S(1)]$, are quite distinct between the two regions, even with a temperature difference of only 500 K.

For comparison, in Table 1 we also show models of low-density fluorescence ($n_H = 10^4$ cm^{-3} , $\chi = 10^2$, $T_0 = 500$ K) and thermal excitation indicative of a shock ($T = 2000$ K, Black & van Dishoeck 1987). We have obtained additional K-band spectra towards the BNKL nebula to compare to the shock model. If we disregard the weak, large-scale emission in transitions of $v \geq 3$ observed in Orion (Luhman et al. 1994), the dereddened line ratios ($A_K = 1$) for BNKL match exactly with those of the thermal model in Table 1. However, the corrected line ratios observed towards the bar and Orion S do not match the thermal model, demonstrating that shocks cannot dominate the H_2

emission in these regions. While a dense PDR and a shock produce a similar ratio of $F[2-1\text{ S}(1)]/F[1-0\text{ S}(1)]$, the strengths of 1-0 Q(1) and 1-0 Q(2), in addition to several weaker transitions shown in Table 1, relative to 1-0 S(1) clearly discriminate between the two excitation mechanisms. The low-density model shown in Table 1, which is insensitive to changes in χ , also fails to match any of the observed spectra for the bar and Orion S. In fact, virtually all of the H_2 emission, even the $v = 2$ and 3 transitions, is accounted for by a dense PDR without the need for a diffuse, pure fluorescent component, the implications of which are explored in § 4.1.3. The fluorescent transitions at J and H predicted by the favored models in Table 1 (under no extinction) fall below our detection limits, which were 20% (J) and 5-10% (H) of 1-0 S(1) at Bar2 and Orion S and 30% (J) and 20% (H) of 1-0 S(1) at Bar1. In low-resolution ($R = 950$) K-band long-slit spectra of the bar, Marconi et al. (1997) have recently measured several 1-0 and 2-1 lines with marginal detections of a few $v = 3$ transitions. Relying on the ratio of 2-1 S(1)/1-0 S(1), they estimate a density of $n_{\text{H}} = 3 - 6 \times 10^4 \text{ cm}^{-3}$ and thus conclude that there is no evidence for a substantial filling factor of dense clumps. This is in direct contrast to our results, where we find excellent agreement between the observed line ratios of the strongest 16 K-band H_2 transitions and the predicted values for a dense PDR ($n_{\text{H}} = 10^6 \text{ cm}^{-3}$).

Finally, we examine the observed and predicted surface brightness of the H_2 emission. For Bar1, Bar2, and Orion S, we measure $I[1-0\text{ S}(1)] = 0.71 \pm 0.14$, 1.8 ± 0.4 , and $(2.6 \pm 0.5) \times 10^{-4} \text{ erg s}^{-1} \text{ cm}^{-2} \text{ sr}^{-1}$. If we correct for the reddening ($A_{\text{K}} \sim 1$) of the layer between the ionization front (IF) and H_2 emission region (see § 4.1.4), we arrive at $I[1-0\text{ S}(1)] = 1.8$, 4.5, and $6.5 \times 10^{-4} \text{ erg s}^{-1} \text{ cm}^{-2} \text{ sr}^{-1}$. The surface brightnesses predicted by the face-on models in Table 1 are 1.4, 4.7, and $12 \times 10^{-4} \text{ erg s}^{-1} \text{ cm}^{-2} \text{ sr}^{-1}$ for Bar1, Bar2, and Orion S. If we include the effect of inclination, the model surface brightnesses are up to an order of magnitude greater than the dereddened, observed values. Since these PDR model predictions only apply to the dense component of the PDR ($n_{\text{H}} \sim 10^6 \text{ cm}^{-3}$), a clump filling factor less than unity (10-50%) could bring the observed and theoretical surface brightnesses into agreement.

4.1.3. *The Source of the H_2 Spectrum*

In one of the first models of the bar, Hayashi et al. (1985) suggested that the near-IR H_2 emission originated from shocked material ($T = 2000 \text{ K}$) along the edge of the expanding H II region, with low-density fluorescent emission dominating beyond the bar, deeper into the molecular cloud. However, Tielens et al. (1993) and van der Werf et al. (1996) concluded that shocks are not an important contributor to the H_2 emission since the large

shock velocities necessary ($> 10 \text{ km s}^{-1}$) are not observed (although they could be hidden by the inclination of the bar) and are not expected in an evolved H II region. Instead, various authors have proposed a two-component PDR as the source of the H_2 emission in the bar. Tauber et al. (1994) and Hogerheijde et al. (1995) found clumps on the scale of $10''$ and smaller, which they interpreted as dense regions ($n_{\text{H}} \gtrsim 10^6 \text{ cm}^{-3}$) of low filling factor within a diffuse interclump medium ($n_{\text{H}} \sim 10^4 \text{ cm}^{-3}$). The dense clumps would then produce the thermal H_2 spectrum with the low-density material responsible for the emission in 2-1 S(1), which was assumed to be fluorescent. Our measurements of this transition relative to 1-0 S(1) towards the Bar1 and Bar2 apertures are consistent with those of other studies (Omodaka et al. 1994; Usuda et al. 1996; van der Werf et al. 1996). Most recently, to account for the ratio of $F[2-1 \text{ S}(1)]/F[1-0 \text{ S}(1)] \sim 0.33$ behind the bar (equivalent to our Bar1 aperture), van der Werf et al. (1996) concluded that a diffuse medium ($n_{\text{H}} \sim 10^4 \text{ cm}^{-3}$) of fluorescent H_2 produces the 2-1 S(1) emission in this region. However, as demonstrated in § 4.1.2, we find that the entire H_2 spectrum, including $v = 2$ and 3 transitions, is reproduced by a dense PDR towards both the Bar1 and Bar2 apertures. Contrary to previous suggestions, shocked emission at the H_2 peak (Bar2) and low-density fluorescence behind the bar (Bar1) cannot account for the observed line ratios. In moving across the bar away from the ionizing stars (Bar2 to Bar1), it appears that a dense PDR continues to dominate the H_2 emission as the temperature slowly decreases.

Data from far-IR to millimeter wavelengths imply the presence of a young stellar object 1'.5 south of IRc2, referred to as Orion S (McMullen, Mundy, & Blake 1993, references therein). While no counterpart has been detected at shorter wavelengths, prominent emission is apparent in the immediate vicinity of Orion S in optical transitions (Pogge, Owen, & Atwood 1992), $\text{Br}\gamma$, 1-0 S(1), and 2-1 S(1) (Usuda et al. 1996). In measurements of [S II] emission, Pogge et al. (1992) derived significantly higher densities towards Orion S than in the bar, consistent with the difference in densities between the two regions we find from [Fe II] (see § 4.3). Pogge et al. (1992) interpreted the Orion S emission as arising from a dense IF and PDR at the back of the blister H II region. On the other hand, Usuda et al. (1996) found a thermal ratio of $F[2-1 \text{ S}(1)]/F[1-0 \text{ S}(1)] = 0.1$, similar to what we observe, and suggested that the H_2 emission originates in shocked material from the unseen, embedded young stellar object. However, as demonstrated in § 4.1.2, the overall K-band H_2 spectrum clearly originates in a dense PDR rather than shocked material. The stratification of the various species in Figure 2 is also similar to what we observe towards the bar, further supporting the inclined PDR nature of the Orion S emitting region. Compared to the bar, the spatial distributions of these species imply a smaller inclination and more face-on orientation in Orion S, which is consistent with the somewhat lower extinction observed in the H_2 spectrum of the latter.

4.1.4. *The Effect of Clumps on PDR Structure*

Hogerheijde et al. (1995) proposed a model for the bar where the PDR is face-on towards the ionized gas, edge-on at the emission ridge of the bar, and face-on again southeast of the bar. Furthermore, Tauber et al. (1994) and Hogerheijde et al. (1995) found that clumps do not affect the PDR structure substantially. Although van der Werf et al. (1996) adopted the geometry proposed by Hogerheijde et al. (1995), the former concluded that clumps play an important role in determining the PDR thickness due to the large clump area filling factor of 50%, corresponding to an area filling factor of 25% as seen by the Trapezium stars. This suggestion by van der Werf et al. (1996) may provide a natural explanation for one of the primary departures of the observed bar structure from that of standard PDR models: the anomalous position of the H₂ emission region relative to the IF. In Figure 1 we see that the H₂ emission reaches a maximum $\sim 15''$ beyond the O I emission, which traces the IF. This fact has been demonstrated previously through other observations of the H₂ emission region (Parmar, Lacy, & Achtermann 1991) and the IF (van der Werf et al. 1996; Omodaka et al. 1994). Nearly coincident with the IF is a ridge of dust emission features at 3.3 μm (Sellgren et al. 1990) and 10 μm (Becklin et al. 1976). As discussed in detail by Omodaka et al. (1994), in a homogeneous PDR the UV photons should be absorbed by dust within a thin layer of $A_K \sim 0.1$ at the outer edge of the IF where emission in both the dust and H₂ is expected to arise, but instead the H₂ emission occurs at a position 15'' beyond the IF. Wyrowski et al. (1997) have also noted a similar anomaly in observations of C91 α towards the bar. Whereas standard PDR models (Tielens & Hollenbach 1985) predicted the H₂ emission to arise in a layer between the IF and C91 α , Wyrowski et al. (1997) found that the H₂ is coincident with the carbon emission. Both Omodaka et al. (1994) and Wyrowski et al. (1997) suggested that the displacement of the H₂ emission peak relative to other species may be explained by either shock excitation of the H₂ or a clumpy PDR in which UV photons can penetrate the large depth observed between the IF and H₂ emission region.

Our observations provide further compelling evidence that the H₂ emission arises well beyond the IF. As discussed in § 4.1.1, after correcting for the extinction towards the ionized gas (and presumably the IF) and using three pairs of H₂ transitions with common upper levels, we derive extinctions of $A_K \sim 2.6$ and 2.3 towards the H₂ peak (Bar2) and the weaker H₂ emission beyond the bar (Bar1). An internal extinction of $A_K \sim 1$ would be apparent in the spectrum if the PDR is inclined nearly edge-on, but the remaining reddening of $A_K \sim 1-1.5$ must be due to material between the IF and H₂ emission region. If we adopt a distance to Orion of $d = 450$ pc, $N_{\text{H}}/A_V \sim 2 \times 10^{21} \text{ mag}^{-1} \text{ cm}^{-2}$ (Bohlin, Savage, & Drake 1978), and a plausible average density ($n_{\text{H}} \sim 2-3 \times 10^5 \text{ cm}^{-3}$), then the optical depth of this 15'' layer is consistent with the extinction we measure towards the H₂ emission

region. Since we have shown that the H₂ spectrum towards the bar is only reproduced by a dense PDR and not a shock (see § 4.1.2), we conclude that a significant amount of UV radiation is penetrating deep into the atomic gas, probably due to a PDR with a significant clump filling factor. This is consistent with the results of van der Werf et al. (1996), who found large clumps on the size of $\sim 10''$. Since this is of order the width of the H₂ peak on the bar, it is not surprising that clumpiness is not obvious in the distribution of 1-0 S(1) emission we observe across the bar. On the other hand, the dominance of H₂ fluorescent emission several arcminutes from the Trapezium stars implies a low clump filling factor for these distant regions (Luhman et al. 1994). Hence, the low filling factor ($\sim 1\%$) assumed by Luhman et al. (1997) may be appropriate in their study of the large-scale H₂ emission across the Orion A molecular ridge, in contrast to the higher clump filling factor implied by our data in the bar and Orion S regions.

4.2. Helium Lines

Systematic errors in telluric correction of emission-line spectra are often overlooked, especially in the previous observations of emission in He 2¹P – 2¹S 2.0587 μm . For instance, we find that the flux in this line in 1996 October is 60% of the value measured in 1995 December, as determined by comparing the ratio of F(He 2.0587 μm)/F(Br γ) at each date. The model shown in Figure 6 predicts a ratio of 0.43, which is fairly close to the measured value considering the sensitivity of this ratio to the velocities and line widths. A value of 0.60 is produced by the model by simply increasing the V_{obs} by 3 km s⁻¹ and using FWHM = 25 km s⁻¹. Due to these telluric line effects and the complex and uncertain fluorescent excitation of this transition (Shields & DePoy 1994), the 2¹P – 2¹S 2.0587 μm emission line is not considered further in our analysis.

In addition to the prominent line at 2.0587 μm , we have observed ~ 30 other He I transitions in our spectra, most of which have not been detected previously. Most of the lines in the n^{3,1}F – 4^{3,1}D series, appearing at the blue side of the Brackett lines, are quite weak, yet apparent in our spectra. Note that these H-band transitions were labeled as unidentified in similar spectra of Hubble 12 (Luhman & Rieke 1996). Since the 11^{3,1}F – 4^{3,1}D 1.6780, 1.6786 μm lines are blended with strong [Fe II] emission, these transitions are omitted from the following analysis. The 7^{3,1}L – 4^{3,1}F 2.1648 μm feature is visible in the wing of Br γ , but we cannot measure its strength reliably and omit it from our discussion as well. In Table 2, we present the fluxes of the remaining He I transitions relative to the 4³D – 3³P 1.7007 μm line for the Orion S and Bar3 positions. As an additional test of the He I models, line ratios are given for Hubble 12 (Hora & Latter 1996; Luhman & Rieke 1996) and the ultra-compact

H II region G45.12+0.13 (Lumsden & Puxley 1996). We compare these line ratios to the predictions of Smits (1996) for collisional excitation with $T_e = 5000, 10000, \text{ and } 20000$ K at $n_e = 10^4 \text{ cm}^{-3}$. These theoretical line ratios are insensitive to electron density. In the least-squares sense, we find that the data are fit equally well with model predictions at $T_e = 10000$ and 20000 K.

In the four sources in Table 2, most transitions have observed line ratios which compare well with predicted values. Exceptions include $4^3\text{P} - 3^3\text{S}$ $1.2531 \mu\text{m}$ and $7^3\text{P} - 4^3\text{S}$ $1.7455 \mu\text{m}$ (after correction for blended H_2 and $[\text{Fe II}]$), which are too strong relative to the model predictions for each source in question. As discussed by Lumsden & Puxley (1996) regarding G45.12+0.13, optically thick UV transitions in $n^3\text{P} - 2^3\text{S}$ can lead to highly populated $n^3\text{P}$ levels, which would enhance any transitions from such levels. Under optically thick conditions, Robbins (1968) and Lumsden & Puxley (1996) calculated similar enhancement values ranging from ~ 4 to ~ 2 for the transitions with upper levels of 4^3P to 7^3P , respectively. All detected transitions from $n^3\text{P}$ in the compact H II regions Hubble 12 ($4^3\text{P} - 3^3\text{S}$, $5^3\text{P} - 3^3\text{D}$, $7^3\text{P} - 4^3\text{S}$, $6^3\text{P} - 4^3\text{S}$, $7^3\text{P} - 4^3\text{D}$) and G45.12+0.13 ($4^3\text{P} - 3^3\text{S}$, $5^3\text{P} - 3^3\text{D}$, $7^3\text{P} - 4^3\text{S}$) have strengths consistent with these predictions. In the more evolved and extended H II region in Orion, we find that $4^3\text{P} - 3^3\text{S}$ is clearly stronger than model predictions of Smits (1996), but only by a factor of ~ 1.5 , much less than in Hubble 12 and G45.12+0.13. It is therefore not surprising that most of the remaining higher level transitions from $n^3\text{P}$ levels are consistent with little or no enhancement. The only obvious exception is the transition in $7^3\text{P} - 4^3\text{S}$ $1.7455 \mu\text{m}$, which is very strong compared to model predictions of Smits (1996) even after subtraction of the expected contribution of $[\text{Fe II}]$ $1.7454 \mu\text{m}$. This feature may include a third unidentified line blended with He I and $[\text{Fe II}]$, possibly C I at $1.7453 \mu\text{m}$ (Outred 1978). We do not expect fluorescent emission in H_2 7-5 Q(3) at $1.7463 \mu\text{m}$ to contribute significantly to this blend in the Orion bar or Orion S. In conclusion, it appears that the transitions in $n^3\text{P} - 2^3\text{S}$ are optically thick in Hubble 12 and G45.12+0.13, while the effect is less extreme in Orion. This opacity effect may explain the anomalous decrement in these UV transitions reported by Martin et al. (1996) in observations of Orion.

4.3. Iron Lines

We have detected numerous near-IR $[\text{Fe II}]$ and $[\text{Fe III}]$ lines in the Bar3 and Orion S apertures, which are given relative to the lines at $1.6440 \mu\text{m}$ and $2.2183 \mu\text{m}$ in Tables 3 and 4. As discussed in § 4.2, enhancement in the He I transition at $1.7455 \mu\text{m}$ and the presence of a blended unidentified line are likely, so we cannot reliably measure the flux

of [Fe II] 1.7454 μm . Since several pairs of [Fe II] transitions possess the same upper levels, their relative strengths are determined by the A-values and line wavelengths alone, making them useful for reddening estimates. In practice, since most of these lines are fairly weak and cover short wavelength baselines, the resulting extinction measurements are highly uncertain. However, the two strongest near-IR [Fe II] transitions are substantially separated in wavelength and have the same upper level, with an expected ratio of $F(1.2570 \mu\text{m})/F(1.6440 \mu\text{m}) = 1.36$. Since all line ratios are corrected for the reddening towards the ionized hydrogen through the flux calibration in § 3.1, we therefore derive $A_K \sim 0.3 \pm 0.3$ as the differential line-of-sight extinction between the regions of H II and Fe II in both the bar and Orion S.

In recent years, there has been some question as to the physical conditions, particularly the density, in the Orion [Fe II] emission regions. Bautista, Pradhan, & Osterbrock (1994) and Bautista & Pradhan (1997) examined optical and J-band [Fe II] lines towards Orion, concluding that the emission in [Fe II] is produced from high-density gas ($n_e \sim 2 \times 10^6 \text{ cm}^{-3}$). With improved spectroscopic data and new model calculations, Baldwin et al. (1996) found that the optical [Fe II] line ratios indicated highly-populated upper levels in Fe II, in agreement with observations of Bautista et al. (1994). But the latter authors attributed such level populations to collisional excitation in a dense environment, whereas Baldwin et al. (1996) proposed that UV pumping can also effectively populate the upper levels of Fe II in a low-density gas ($n_e \sim 10^4 \text{ cm}^{-3}$).

Since the IR transitions in [Fe II] occur between lower levels, these line ratios are insensitive to continuum pumping and depend only on collisional excitation. Therefore, the IR [Fe II] lines represent an excellent density diagnostic. For instance, Baldwin et al. (1996) noted that the strength of the line at 1.2570 μm (Lowe, Moorehead, & Wehlau 1979) relative to the optical lines implies low densities. Marconi et al. (1997) have also used the strength of one [Fe II] line relative to the transition at 1.6440 μm , which was completely blended with Br12 at their resolution ($R = 700$), to estimate a density of $n_e \sim 10^4 \text{ cm}^{-3}$ towards the bar. However, with the large number of J- and H-band [Fe II] lines that we have observed towards the bar and Orion S, we can perform a much more systematic measurement of the density, similar to that done for Hubble 12 and the starburst galaxy NGC 253 (Luhman & Rieke 1996; Engelbracht et al. 1997). In Table 3 we compare the observed line ratios with those predicted by the collisional model predictions of Bautista & Pradhan (1996) for $n_e = 10^3, 10^4$, and 10^6 cm^{-3} at $T_e = 10^4 \text{ K}$. The J-band transitions are consistent within the uncertainties with all three models, while the H-band lines indicate densities of $n_e \sim 10^4 \text{ cm}^{-3}$ for Orion S and $n_e \sim 10^3\text{-}10^4 \text{ cm}^{-3}$ for the bar. K-band emission in [Fe III] is also strong towards Orion, as noted by DePoy & Pogge (1994) in their observations of the Orion S region. We have measured four near-IR [Fe III] transitions and compared the

line ratios to the model predictions of Keenan et al. (1992). As shown in Table 4, the line ratios are all roughly consistent with the values predicted for $n_e \sim 10^4 \text{ cm}^{-3}$. The differing density measurements derived in the optical and IR can be explained in a model where the near-IR emission arises in low-density, fully-ionized material while the optical transitions are produced predominantly in high-density, partially-ionized regions, as proposed by Bautista & Pradhan (1997).

4.4. Other Lines

There are three moderately strong unidentified emission lines in our spectra of the bar and Orion S. A feature appears at $2.1987 \mu\text{m}$ which has been observed in the spectra of Hubble 12 and other planetary nebulae (Luhman & Rieke 1996; Hora & Latter 1996). A second unidentified line, which apparently has never been detected before, is visible at $2.2245 \mu\text{m}$ and is partially blended with 1-0 S(0) $2.2233 \mu\text{m}$ in the spectrum of Orion S in Figure 5. The line does not appear towards Bar2 but is clearly resolved from weak 1-0 S(0) $2.2233 \mu\text{m}$ emission in the Bar3 spectrum. Consequently, both of these unidentified emission lines appear to arise from atomic species since they are only detected towards the H II regions in Orion and Hubble 12. In preparation for the observations presented here, we obtained low-resolution ($R = 1200$) spectra of the bar and Orion S at J, H, and K. In the J-band spectrum, which extended to shorter wavelengths than the moderate-resolution spectrum, we detect the He I transition at $1.1973 \mu\text{m}$ and an unidentified line at $1.1889 \pm 0.0002 \mu\text{m}$. Possible line identifications include C I ($1.1896 \mu\text{m}$) and Si I ($1.188 \mu\text{m}$). An emission line at a similar wavelength is also detected in the starburst galaxies NGC 253 (Engelbracht et al. 1997) and NGC 6240 (Engelbracht, Rieke, & Rieke 1998; Kulesa et al. 1998).

5. Conclusion

We have presented near-IR spectra ($R \sim 3000$) which provide new insight into the physical conditions and excitation mechanisms present in the Orion bar and Orion S regions:

1. After comparing the relative strengths of 16 H_2 lines to those produced by models of dense PDRs (Draine & Bertoldi 1996) and thermal excitation, we rule out shocks as a significant contributor to emission in either the bar or Orion S. While similar ratios of $F[2-1 \text{ S}(1)]/F[1-0 \text{ S}(1)]$ arise in dense PDRs and shocks, we demonstrate that

several other H_2 lines in our data are powerful diagnostics in distinguishing between the two excitation mechanisms. Towards the peak of H_2 emission on the bar, the line ratios are in excellent agreement with PDR model predictions ($n_{\text{H}} = 10^6 \text{ cm}^{-3}$, $\chi = 10^5$, $T_0 = 1000 \text{ K}$). In the region behind the bar and away from the ionizing stars, the entire H_2 spectrum, including the transitions with $v = 2$ and 3, implies the same density regime but with a lower temperature ($T_0 = 500 \text{ K}$) and UV field strength ($\chi = 10^4$). This is in contrast to previous suggestions that low-density fluorescing material is required to produce the observed 2-1 S(1) emission. In the Orion S region, the H_2 line ratios reveal the presence of a dense PDR similar to that of the bar, but with a higher temperature ($T_0 = 1500 \text{ K}$) in Orion S. The spatial stratification of several species (O I, H I, [Fe II], [Fe III], H_2) is similar between the bar and Orion S, indicating an inclined PDR in each region. The geometrical enhancement of line emission observed in these two sources may be a common phenomenon in other bright regions of the ISM as well.

2. Using three pairs of H_2 lines with common upper levels, we derive the extinction towards the H_2 emission regions in the bar ($A_{\text{K}} = 2.6 \pm 0.7$) and Orion S ($A_{\text{K}} = 2.1 \pm 0.5$). Since an edge-on PDR should exhibit a reddening of only $A_{\text{K}} \sim 1$, the remaining extinction is apparently due to a thick layer ($A_{\text{K}} = 1\text{-}1.5$) of material between the ionization front and the H_2 emitting gas. While this layer is predicted to be rather thin ($A_{\text{K}} \sim 0.1$) in homogeneous PDR models, a significant filling factor of dense clumps ($n_{\text{H}} \sim 10^6 \text{ cm}^{-3}$) could allow UV photons to penetrate further into the PDR and produce the H_2 peak at the large depth we observe in the bar and Orion S.
3. Most of the ~ 30 He I emission lines have relative strengths consistent with models of collisional excitation (Smits 1996). A few transitions, particularly $4^3\text{P} - 3^3\text{S}$ $1.2531 \mu\text{m}$, appear stronger than predicted, possibly due to opacity in the UV transitions of $n^3\text{P} - 2^3\text{S}$. After comparing the He I line ratios we observed in Orion to those measured in Hubble 12 and G45.12+0.13 (Hora & Latter 1996; Luhman & Rieke 1996; Lumsden & Puxley 1996), we find that this effect is more pronounced in the latter two sources.
4. The line ratios of 10 near-IR [Fe II] transitions agree well with the values predicted by Bautista & Pradhan (1996) for collisional excitation towards the bar ($n_{\text{e}} \sim 10^3\text{-}10^4 \text{ cm}^{-3}$) and Orion S ($n_{\text{e}} \sim 10^4 \text{ cm}^{-3}$). In addition, the relative strengths of four [Fe III] transitions match predictions by Keenan et al. (1992) for a density of $n_{\text{e}} \sim 10^4 \text{ cm}^{-3}$. When these results are combined with measurements of higher densities ($n_{\text{e}} \sim 10^6 \text{ cm}^{-3}$) from optical [Fe II] data, it appears that dense, partially-ionized regions are responsible for the optical emission while fully-ionized

gas dominates the near-IR [Fe II] transitions, which is consistent with recent model predictions of Bautista & Pradhan (1997).

We thank G. Rieke and M. Rieke for help in obtaining the data. We are grateful to M. Bautista, F. Bertoldi, B. Draine, and D. Smits for useful advice and access to their model calculations. We thank P. Martin for communicating results prior to publication and G. Rieke for comments on the manuscript. K. L. acknowledges support from NASA grant NAGW-4083 under the Origins of Solar Systems program. C. E. and M. L. were supported by NSF grant AST95-29190 and the Office of Naval Research, respectively.

REFERENCES

- Baldwin, J. A., et al. 1996, *ApJ*, 468, L115
- Bautista, M. A., & Pradhan, A. K. 1996, *A&AS*, 115, 551
- Bautista, M. A., & Pradhan, A. K. 1997, *ApJ*, in press
- Bautista, M. A., Pradhan, A. K., & Osterbrock, D. E. 1994, *ApJ*, 432, 135
- Becklin, E. E., & Beckwith, S., Gatley, I., Matthews, K., Neugebauer, G., Sarazin, C., & Werner, M. W. 1976, *ApJ*, 207, 770
- Black, J. H, & van Dishoeck, E. F. 1987, *ApJ*, 412, 322
- Bohlin, R. C., Savage, B. D., & Drake, J. F. 1978, *ApJ*, 224, 132
- Burton, M. G., Hollenbach, D. J., & Tielens, A. G. G. M. 1990, *ApJ*, 365, 620
- DePoy, D. L, & Pogge R. W. 1994, *ApJ*, 433, 725
- DePoy, D. L, & Shields, J. C. 1994, *ApJ*, 422, 187
- Draine, B. T., & Bertoldi, F. 1996, *ApJ*, 468, 269 (DB96)
- Engelbracht, C. W., Rieke, M. J, Rieke, G. H., Kelly, D. M., & Achtermann, J. M. 1997, *ApJ*, in press
- Engelbracht, C. W., Rieke, M. J, & Rieke, G. H. 1998, submitted
- Goldschmidt, O., & Sternberg, A. 1995, *ApJ*, 439, 256
- Hayashi, M., Hasegawa, T., Gatley, I., Garden, R., & Kaifu, N. 1985, *MNRAS*, 215, 31
- Hogerheijde, M. R., Jansen, D. J., & van Dishoeck, E. F. 1995, *A&A*, 294, 792
- Hora, J. L., & Latter, W. B. 1996, *ApJ*, 461, 288

- Jansen, D. J., Spaans, M., Hogerheijde, M. R., & van Dishoeck, E. F. 1995, *A&A*, 303, 541
- Johansson, S. 1978, *Physica Scripta*, 18, 217
- Keenan, F. P., Berrington, K. A., Burke, P. G., Zeippen, C. J., Le Dourneuf, M., & Clegg, R. E. S. 1992, *ApJ*, 384, 385
- Kulesa, C. Engelbracht, C. W., Ge, J., & Rieke, G. H. 1998, in prep.
- Livingston, W., & Wallace, L. 1991, An atlas of the solar spectrum in the infrared from 1850 to 9000 cm^{-1} , National Solar Observatory Technical Report 91-001
- Lowe, R. P., Moorehead, J. M., & Wehlau, W. H. 1979, *ApJ*, 228, 191
- Luhman, K. L., & Rieke, G. H. 1996, *ApJ*, 461, 298
- Luhman, M. L., Jaffe, D. T., Keller, L. D., & Pak, S. 1994, *ApJ*, 436, 185
- Luhman, M. L., Jaffe, D. T., Sternberg, A., Herrmann, F., & Poglitsch, A. 1997, *ApJ*, 482, 298
- Lumsden, S. L., & Puxley, P. J. 1996, *MNRAS*, 281, 493
- Maiolino, R., Rieke, G. H., & Rieke, M. J. 1996, *AJ*, 111, 537
- Marconi, A., Testi, L., Natta, A., & Walmsley, C. M. 1997, *A&A*, in press
- Martin, P. G., Rubin, R. H., Ferland, G. J., Dufour, R. J., O'Dell, C. R., Baldwin, J. A., Hester, J. J., & Walter, D. K. 1996, *BAAS*, 28, 106.01
- Martin, W. C. 1973, *J. Phys. Chem. Ref. Data*, 2, 257
- McMullen, J. P., Mundy, L. G., & Blake, G. A. 1993, *ApJ*, 405, 599
- O'Dell, C. R. 1994, *A&AS*, 216, 267
- Omodaka, T., Hayashi, M., Hasegawa, T., & Hayashi, S. S. 1994, *ApJ*, 430, 256
- Outred, M. 1978, *J. Phys. Chem. Ref. Data*, 7, 1
- Parmar, P. S., Lacy, J. H., & Achtermann, J. M. 1991, *ApJ*, 372, L25
- Pogge, R. W., Owen, J. M., & Atwood, B. 1992, *ApJ*, 399, 147
- Rieke, G. H., & Lebofsky, M. J. 1985, *ApJ*, 288, 618
- Robbins, R. R. 1968, *ApJ*, 151, 511
- Schmid-Burgk, J., Güsten, R., Mauersberger, R., Schulz, A., & Wilson, T. L. 1990, *ApJ*, 362, L25
- Sellgren, K., Tokunaga, A. T., & Nakada, Y. 1990, *ApJ*, 349, 120
- Smits, D. P. 1996, *MNRAS*, 278, 683

- Storey, P. J., & Hummer, D. G. 1995, *MNRAS*, 272, 41
- Sternberg, A., & Dalgarno, A. 1989, *ApJ*, 338, 197
- Sternberg, A., & Dalgarno, A. 1995, *ApJS*, 99, 565
- Sugar, J., & Corliss, C. 1985, *J. Phys. Chem. Ref. Data*, 14, Suppl. 2
- Tauber, J. A., Tielens, A. G. G. M., Meixner, M., & Goldsmith, P. F. 1994, *ApJ*, 422, 136
- Tielens, A. G. G. M., & Hollenbach, D. 1985, *ApJ*, 291, 722
- Tielens, A. G. G. M., Meixner, M. M., van der Werf, P. P., Bregman, J., Tauber, J. A., Stutzki, J., & Rank, D. 1993, *Science*, 262, 86
- Usuda, T., Sugai, H., Kawabata, H., Inoue, M. Y., Kataza, H., & Tanaka, M. 1996, *ApJ*, 464, 818
- van der Werf, P. P., Stutzki, J., Sternberg, A., & Krabbe A. 1996, *A&A*, 313, 633
- Wilson, T. L., & Mauersberger, R. 1991, *A&A*, 244, L33
- Williams, D., Thompson, C. L., Rieke, G. H., & Montgomery, E. F. 1993, *ProcSPIE*, 1308, 482
- Wyrowski, F., Schilke, P., Hofner, P., & Walmsley, C. M. 1997, *ApJ*, 487, L171
- Ziurys, L. M., Martin, R. N., Pauls, T. A., & Wilson, T. L. 1981, *A&A*, 104, 288

Table 2. He Line Ratios^a

$\lambda_{\text{vac}}(\mu\text{m})^c$	transition	Observed				Model ^b		
		Bar3	Orion S	Hubble 12 ^d	G45.12+0.13 ^e	T ₃ = 5	T ₃ = 10	T ₃ = 20
1.2531	4 ³ P – 3 ³ S	0.64 ± 0.10	0.87 ± 0.09	1.42 ± 0.10	1.38 ± 0.08	0.36	0.44	0.56
1.2789,93	5 ^{3,1} F – 3 ^{3,1} D	2.44 ± 0.15	2.61 ± 0.20	2.37±?	5.40 ± 2.00	3.49	3.06	2.67
1.2850	5 ³ S – 3 ³ P	0.11 ± 0.11	0.31 ± 0.11	0.08	0.12	0.18
1.2972	5 ¹ D – 3 ¹ P	0.11 ± 0.11	0.13 ± 0.10	0.52 ± 0.05 ^f	0.52 ± 0.05 ^f	0.23	0.23	0.24
1.2989	5 ³ P – 3 ³ D	0.17 ± 0.11	0.14 ± 0.10	0.10	0.13	0.16
1.5088 ^g	4 ¹ P – 3 ¹ S	0.05 ± 0.06	0.09 ± 0.04	0.23 ± 0.03	0.19 ± 0.05	0.15	0.18	0.21
1.5678,82	15 ^{3,1} F – 4 ^{3,1} D	0.02 ± 0.02	0.05 ± 0.02	0.02 ± 0.02	...	0.02	0.02	0.02
1.5857,62	14 ^{3,1} F – 4 ^{3,1} D	0.01 ± 0.02	0.03 ± 0.02	0.02 ± 0.02	...	0.04	0.04	0.03
1.6085,90	13 ^{3,1} F – 4 ^{3,1} D	0.02 ± 0.02	0.04 ± 0.02	0.02 ± 0.02 ⁱ	...	0.05	0.04	0.04
1.6165	11 ³ D – 4 ³ P	0.02 ± 0.02	0.03 ± 0.02	0.02	0.02	0.02
1.6382,88	12 ^{3,1} F – 4 ^{3,1} D	0.04 ± 0.02	0.06 ± 0.02	0.05 ± 0.01	...	0.06	0.06	0.05
1.6678	10 ³ D – 4 ³ P	0.01 ± 0.01	0.01 ± 0.02	0.04 ± 0.01	...	0.02	0.02	0.02
1.7007	4 ³ D – 3 ³ P	1.00	1.00	1.00	...	1.00	1.00	1.00
1.7334,40	10 ^{3,1} F – 4 ^{3,1} D	0.15 ± 0.04	0.11 ± 0.02	0.08 ± 0.03 ⁱ	...	0.10	0.09	0.09
1.7428	9 ³ D – 4 ³ P	0.04 ± 0.02	0.02 ± 0.01	0.02 ± 0.02	...	0.03	0.03	0.03
1.7455 ^h	7 ³ P – 4 ³ S	0.15 ± 0.05	0.11 ± 0.04	0.14 ± 0.02 ⁱ	0.10 ± 0.05	0.02	0.03	0.03
2.0430	6 ³ P – 4 ³ S	0.03 ± 0.02	0.02 ± 0.03	0.06 ± 0.01	...	0.03	0.03	0.04
2.0587	2 ¹ P – 2 ¹ S	8.08 ± 0.33	5.13 ± 0.16	4.65 ± 0.11	11.00 ± 0.70
2.1127,38	4 ^{3,1} S – 3 ^{3,1} P	0.40 ± 0.04	0.34 ± 0.03	0.53 ± 0.02	0.48 ± 0.05	0.25	0.34	0.49
2.1613,22	7 ^{3,1} F – 4 ^{3,1} D	0.23 ± 0.04	0.25 ± 0.03	0.27 ± 0.02	...	0.29	0.27	0.24
2.1821	7 ³ P – 4 ³ D	0.02 ± 0.02	0.03 ± 0.01	0.04 ± 0.02	...	0.02	0.02	0.03
2.1846	7 ¹ D – 4 ¹ P	0.01 ± 0.02	0.02 ± 0.01	0.02 ± 0.02	...	0.02	0.02	0.02

^aLine ratios are relative to 4³D – 3³P 1.7007 μm . For Bar3 and Orion S, $F(\text{He } 1.7007 \mu\text{m})/F(\text{Br}\gamma) = 0.116 \pm 0.005$ and 0.112 ± 0.004 where $F(\text{Br}\gamma) = (4.4 \pm 0.5) \times 10^{-12} \text{ erg s}^{-1} \text{ cm}^{-2}$ and $(1.5 \pm 0.2) \times 10^{-11} \text{ erg s}^{-1} \text{ cm}^{-2}$.

^bSmits (1996) with $n_e = 10^4 \text{ cm}^{-3}$. Model values for the transition at 2.0587 μm are highly uncertain.

^cMartin (1973).

^dJ-band data from Hora & Latter (1996). H- and K-band data from Luhman & Rieke (1996).

^eLumsden & Puxley (1996).

^fBlended with the transition at 1.2989 μm .

^gThe flux in this line was estimated by assuming the contribution of Br22 is that derived from the measured Br21 flux and the ratio of Br21 to Br22 predicted by case B recombination with $n_e = 10^2 \text{ cm}^{-3}$ and $T_e = 10^4 \text{ K}$ (Storey & Hummer 1995).

^hBlended [Fe II] emission was subtracted by using the theoretical line strength relative to [Fe II] 1.6440 μm (Bautista & Pradhan 1996).

ⁱBlended fluorescent H₂ emission was subtracted by using the theoretical pure fluorescent line strength relative to 1-0 S(1) 2.1220 μm (Black & van Dishoeck 1987).

Table 3. [Fe II] Line Ratios^a

$\lambda_{\text{vac}}^{\text{b}}$	transition	Observed		Model ^c		
		Bar3	Orion S	$n_e=10^3$	$n_e=10^4$	$n_e=10^6$
1.2570	${}^4\text{D}_{7/2} - {}^6\text{D}_{9/2}$	1.10 ± 0.11	1.03 ± 0.11	1.36	1.36	1.36
1.2946	${}^4\text{D}_{5/2} - {}^6\text{D}_{5/2}$	0.16 ± 0.12	$0.36 \pm 0.17\text{bl?}$	0.06	0.19	0.36
1.3209	${}^4\text{D}_{7/2} - {}^6\text{D}_{7/2}$	0.41 ± 0.12	0.46 ± 0.13	0.36	0.36	0.36
1.3281	${}^4\text{D}_{5/2} - {}^6\text{D}_{3/2}$	< 0.14	0.21 ± 0.11	0.04	0.12	0.22
1.5339 ^d	${}^4\text{D}_{5/2} - {}^4\text{F}_{9/2}$	0.13 ± 0.05	0.23 ± 0.05	0.07	0.20	0.38
1.5999	${}^4\text{D}_{3/2} - {}^4\text{F}_{7/2}$	0.03 ± 0.03	0.08 ± 0.03	0.03	0.14	0.31
1.6440	${}^4\text{D}_{7/2} - {}^4\text{F}_{9/2}$	1.00	1.00	1.00	1.00	1.00
1.6642	${}^4\text{D}_{1/2} - {}^4\text{F}_{5/2}$	0.03 ± 0.03	0.05 ± 0.04	0.02	0.08	0.16
1.6773 ^e	${}^4\text{D}_{5/2} - {}^4\text{F}_{7/2}$	0.08 ± 0.04	0.10 ± 0.03	0.05	0.15	0.28
1.7116	${}^4\text{D}_{3/2} - {}^4\text{F}_{5/2}$	0.03 ± 0.02	0.05 ± 0.01	0.01	0.04	0.08

^aLine ratios are relative to ${}^4\text{D}_{7/2} - {}^4\text{F}_{9/2}$ 1.6440 μm . For Bar3 and Orion S, $F([\text{Fe II}] 1.6440 \mu\text{m})/F(\text{Br}\gamma) = 0.109 \pm 0.006$ and 0.090 ± 0.004 where $F(\text{Br}\gamma) = (4.4 \pm 0.5) \times 10^{-12} \text{ erg s}^{-1} \text{ cm}^{-2}$ and $(1.5 \pm 0.2) \times 10^{-11} \text{ erg s}^{-1} \text{ cm}^{-2}$.

^bJohannson (1978).

^cCollisional excitation with $T_e = 10^4 \text{ K}$ (Bautista & Pradhan 1996).

^dBr18 was subtracted by interpolating between Br19 and Br17.

^eHe $11^{3,1}\text{F} - 4^{3,1}\text{D}$ was subtracted by interpolating between He $12^{3,1}\text{F} - 4^{3,1}\text{D}$ and $10^{3,1}\text{F} - 4^{3,1}\text{D}$.

Table 4. [Fe III] Line Ratios^a

$\lambda_{\text{vac}}^{\text{b}}$	transition	Observed		Model ^c		
		Orion S	Bar3	$n_e=10^3$	$n_e=10^4$	$n_e=10^5$
2.1457	$^3\text{G}_3 - ^3\text{H}_4$	0.11 ± 0.11	0.17 ± 0.06	0.10	0.17	0.34
2.2183	$^3\text{G}_5 - ^3\text{H}_6$	1.00	1.00	1.00	1.00	1.00
2.2427	$^3\text{G}_4 - ^3\text{H}_4$	0.34 ± 0.12	0.38 ± 0.07	0.26	0.29	0.38
2.3485 ^d	$^3\text{G}_5 - ^3\text{H}_5$	0.89 ± 0.17	0.77 ± 0.09	0.66	0.66	0.66

^aLine ratios are relative to $^3\text{G}_5 - ^3\text{H}_6$ 2.2183 μm . For Bar3 and Orion S, $F([\text{Fe III}] 2.2183 \mu\text{m})/F(\text{Br}\gamma) = 0.015 \pm 0.001$ and 0.016 ± 0.001 where $F(\text{Br}\gamma) = (4.4 \pm 0.5) \times 10^{-12} \text{ erg s}^{-1} \text{ cm}^{-2}$ and $(1.5 \pm 0.2) \times 10^{-11} \text{ erg s}^{-1} \text{ cm}^{-2}$.

^bSugar & Corliss (1985).

^cCollisional excitation with $T_e = 10^4 \text{ K}$ (Keenan et al. 1992).

^dThe flux in this line was estimated by assuming the contribution of Pf29 is that derived from the measured $\text{Br}\gamma$ flux and the ratio of Pf29 to $\text{Br}\gamma$ predicted by case B recombination with $n_e = 10^2 \text{ cm}^{-3}$ and $T_e = 10^4 \text{ K}$ (Storey & Hummer 1995).

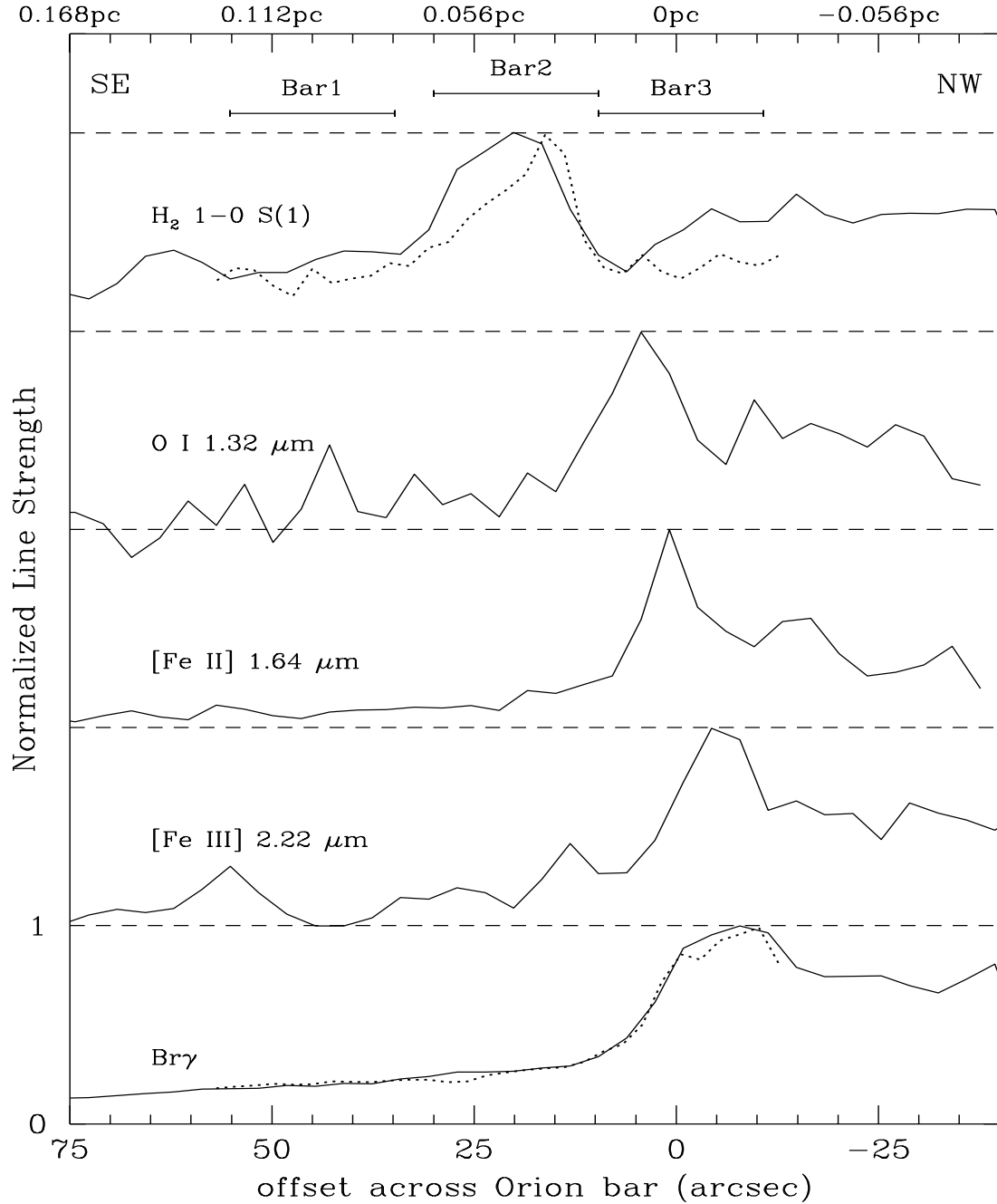


Fig. 1.— Spatial variations of several prominent near-IR emission lines across the Orion bar from SE (left) to NW (right). The solid and dotted profiles are from the data obtained at the 1.55 m and 2.3 m telescopes with each resolution element representing $3''.5 \times 3''.5$ and $2''.4 \times 2''.4$, respectively. Spectra were extracted from apertures indicated by the bars at the top of the figure, referred to as Bar1, Bar2, and Bar3. The origin corresponds to $\alpha = 5^{\text{h}}35^{\text{m}}19^{\text{s}}.5$, $\delta = -5^{\circ}24'53''$ (2000).

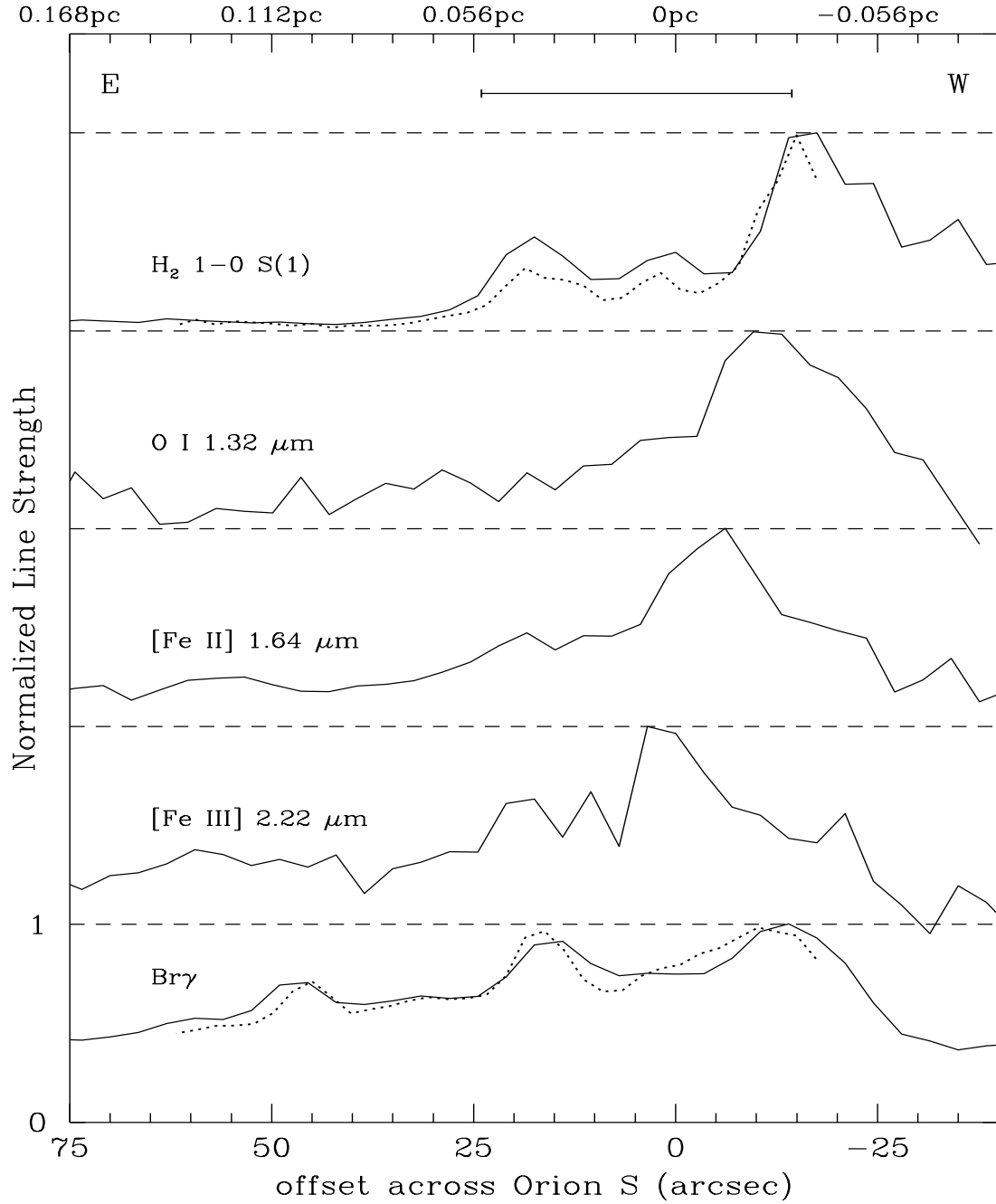


Fig. 2.— Spatial variations of several prominent near-IR emission lines across the Orion S region from E (left) to W (right). The solid and dotted profiles are from the data obtained at the 1.55 m and 2.3 m telescopes with each resolution element representing $3''.5 \times 3''.5$ and $2''.4 \times 2''.4$, respectively. A spectrum was extracted from an aperture indicated by the bar at the top of the figure. The origin corresponds to $\alpha = 5^{\text{h}}35^{\text{m}}15^{\text{s}}.7$, $\delta = -5^{\circ}23'59''$ (2000).

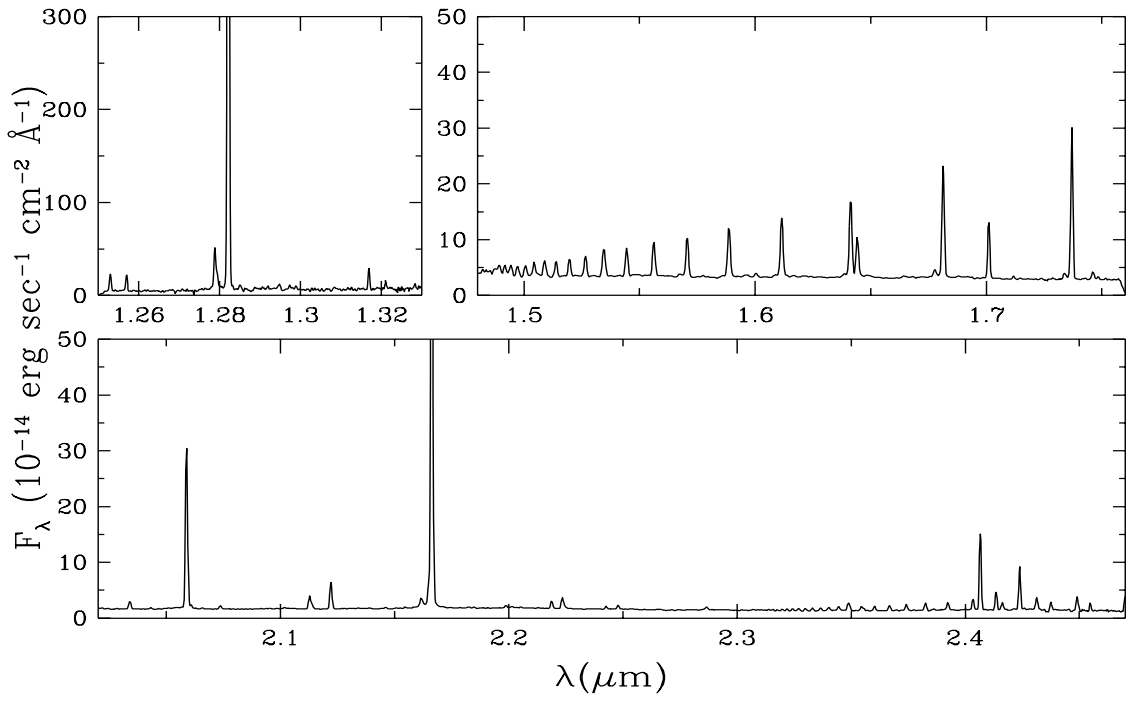


Fig. 3.— The near-IR spectrum of Orion S extracted from the aperture indicated in Figure 2.

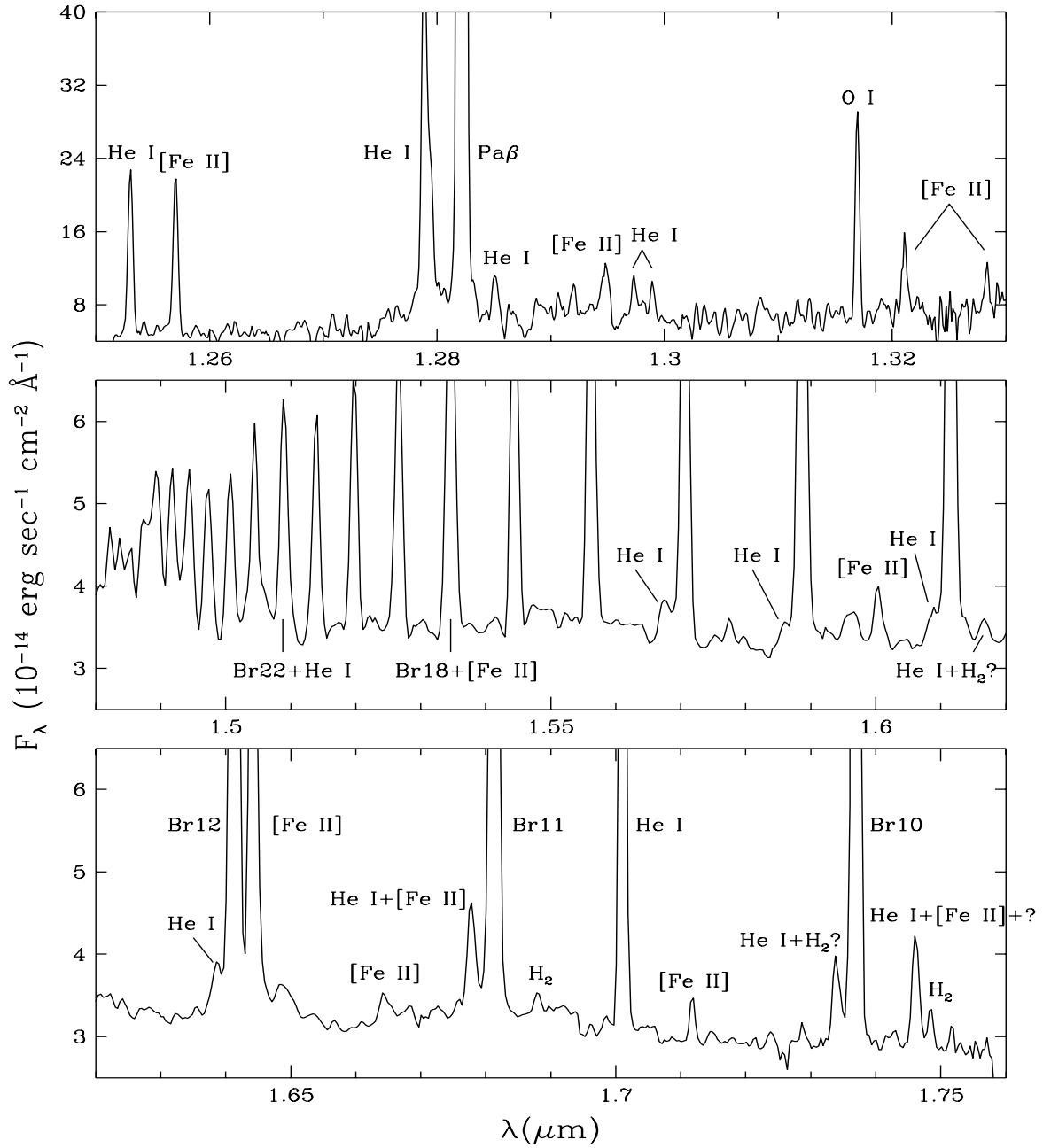


Fig. 4.— The spectrum of Orion S at J and H extracted from the aperture indicated in Figure 2. The flux scales for J and H were derived by using the flux-calibrated K-band spectrum and assuming that $F(\text{Pa}\beta)/F(\text{Br}\gamma)$ and $F(\text{Br lines})/F(\text{Br}\gamma)$ match the values predicted by case B recombination. The unlabeled emission lines between 1.48 and 1.62 μm are Br28 through Br13.

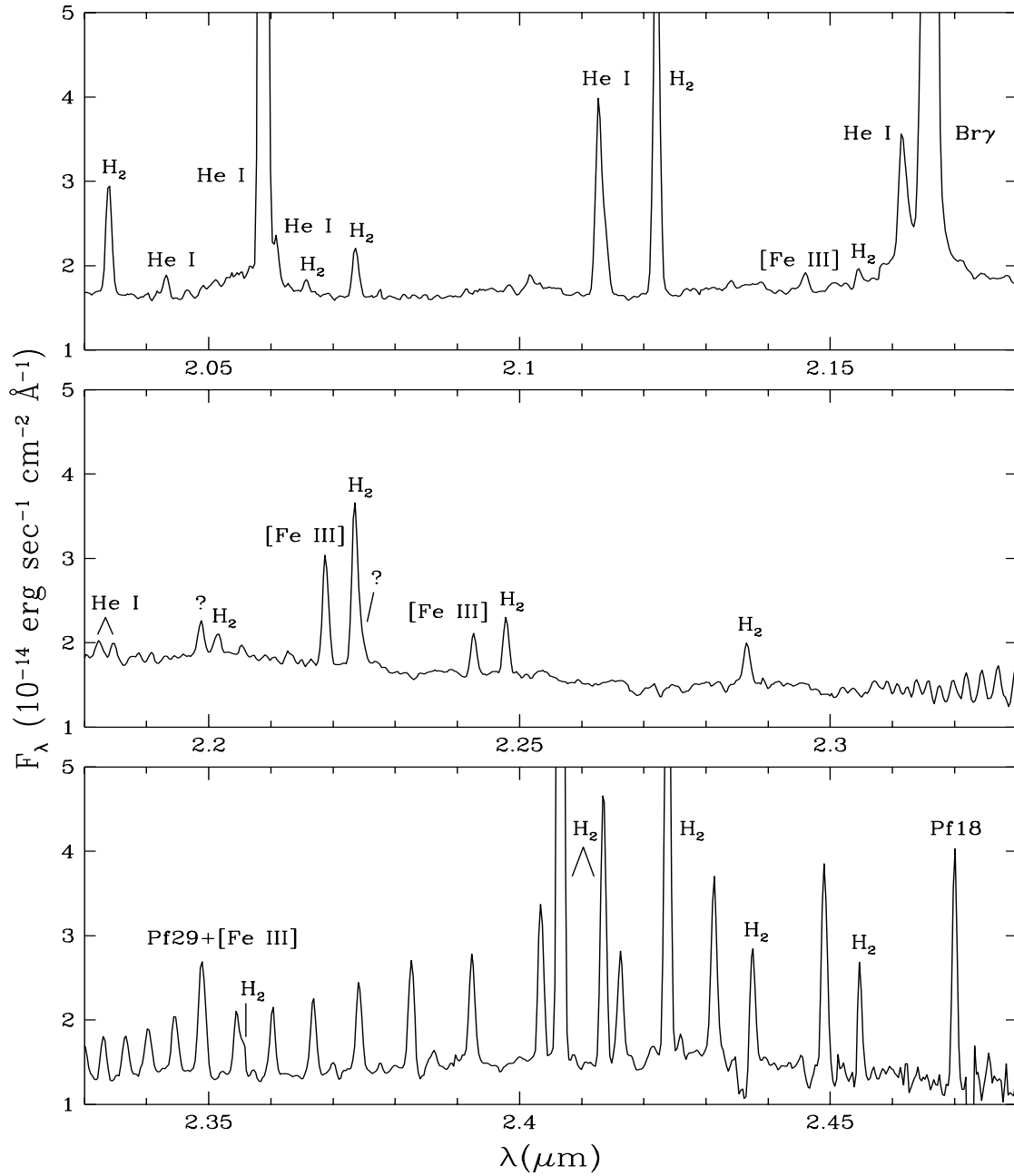


Fig. 5.— The spectrum of Orion S at K extracted from the aperture indicated in Figure 2. The unlabeled emission lines beyond 2.3 μm are Pf45 through Pf19.

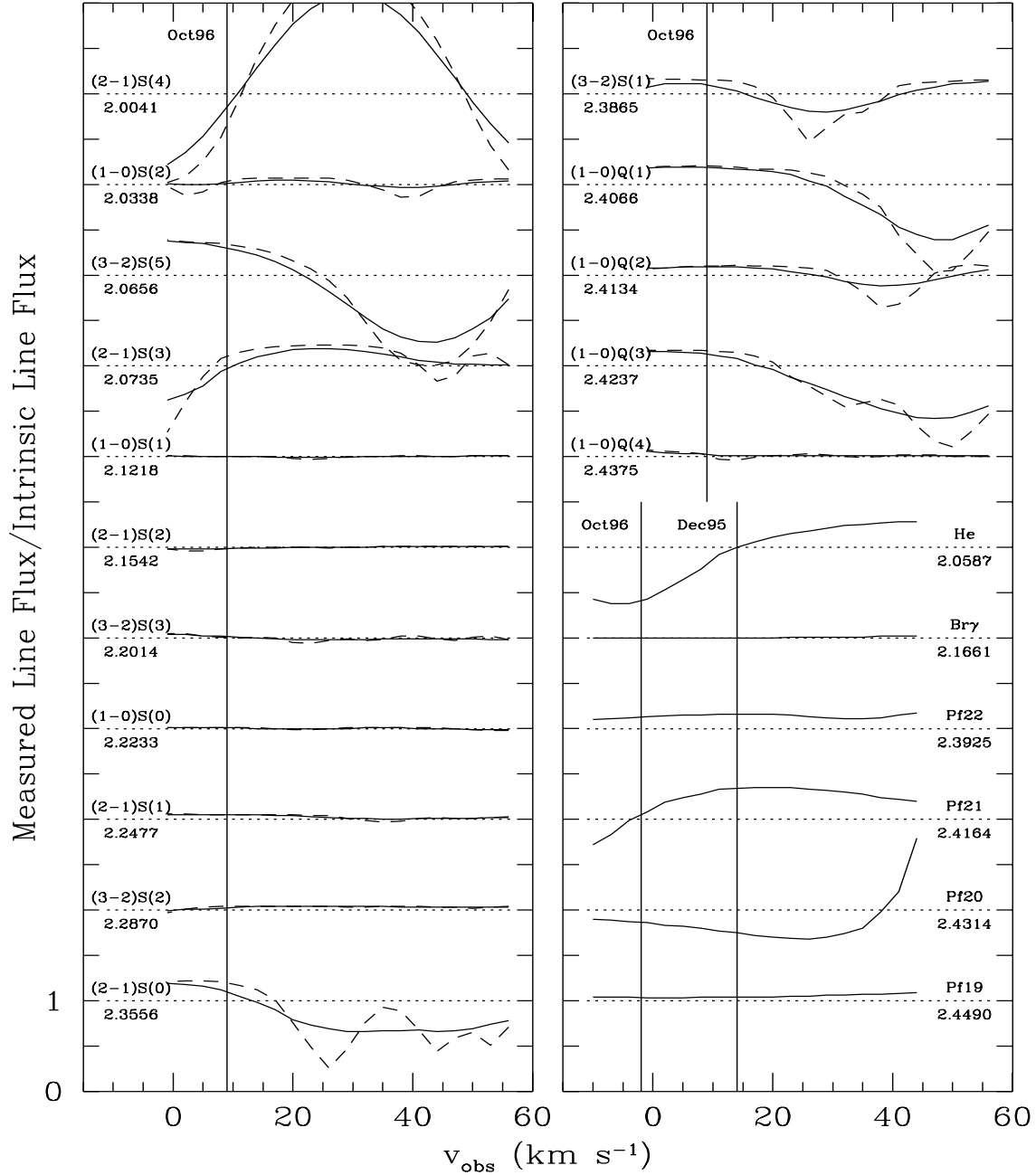


Fig. 6.— To illustrate the effect of imperfect telluric correction, the simulated ratios of measured to intrinsic line fluxes are given for H₂, He, and H lines as a function of observed radial velocities of the emission regions in Orion. An instrumental spectral resolution of $R = 3200$ is assumed with the solid and dashed lines derived with intrinsic FWHMs of 20 and 5 Å, respectively. Estimates of the velocities of the PDR H₂, He, and H regions (taken from the literature) at the dates of our observations are indicated by the vertical lines.

TABLE 1
H₂ LINE RATIOS^a

$\lambda_{\text{vac}}^{\text{b}}$	transition	Observed			Corrected ^c			Model				
		Bar1	Bar2	Orion S	Bar1	Bar2	Orion S	Bar1 ^d	Bar2 ^e	Orion S ^f	low n _H ^g	thermal ^h
2.0338	1-0 S(2)	0.22±0.08	0.27±0.05	0.27±0.03	0.27±0.09	0.33±0.06	0.32±0.04	0.31	0.28	0.26	0.47	0.37
2.0656	3-2 S(5)	0.06±0.04	0.04±0.02	0.02±0.01	0.05±0.04	0.03±0.02	0.02±0.01	0.08	0.06	0.01	0.07	...
2.0735	2-1 S(3)	0.34±0.05	0.19±0.02	0.13±0.02	0.37±0.06	0.21±0.02	0.14±0.02	0.31	0.24	0.06	0.34	0.08
2.1218	1-0 S(1)	1.00	1.00	1.00	1.00	1.00	1.00	1.00	1.00	1.00	1.00	1.00
2.1280	3-2 S(4)	0.06±0.04	0.04±0.02	...	0.06±0.04	0.04±0.02	...	0.04	0.02	0.01	0.05	...
2.1542	2-1 S(2)	0.15±0.08	0.04±0.02	0.04±0.02	0.14±0.07	0.03±0.02	0.03±0.02	0.12	0.09	0.02	0.23	0.03
2.2014	3-2 S(3)	0.12±0.04	0.09±0.03	0.04±0.02	0.11±0.03	0.08±0.02	0.04±0.02	0.11	0.08	0.02	0.16	0.01
2.2233	1-0 S(0)	0.44±0.05	0.40±0.03	0.42±0.03 ⁱ	0.37±0.04	0.33±0.03	0.35±0.03	0.38	0.33	0.30	0.42	0.21
2.2477	2-1 S(1)	0.41±0.05	0.27±0.03	0.12±0.02	0.33±0.04	0.21±0.02	0.10±0.01	0.32	0.24	0.07	0.51	0.08
2.2870	3-2 S(2)	0.05±0.04	0.05±0.02	0.09±0.03	0.04±0.03	0.04±0.01	0.08±0.02	0.04	0.03	0.01	0.11	...
2.3556	2-1 S(0)	0.31±0.05	0.13±0.03	0.07±0.03	0.15±0.05	0.07±0.02	0.04±0.02	0.11	0.07	0.02	0.22	0.02
2.3865	3-2 S(1)	0.19±0.06	0.21±0.03	0.03±0.01	0.11±0.04	0.12±0.02	0.02±0.01	0.11	0.07	0.02	0.26	0.01
2.4066	1-0 Q(1)	2.85±0.25	3.25±0.15	2.57±0.10	1.52±0.15	1.63±0.08	1.43±0.06	1.98	1.58	1.25	0.99	0.70
2.4134	1-0 Q(2)	0.75±0.10	0.73±0.06	0.61±0.03	0.43±0.06	0.40±0.03	0.37±0.02	0.42	0.37	0.33	0.46	0.22
2.4237	1-0 Q(3)	1.24±0.13	1.39±0.09	1.35±0.06	0.67±0.08	0.71±0.05	0.76±0.03	0.70	0.71	0.71	0.70	0.70
2.4375	1-0 Q(4)	...	0.22±0.10	0.23±0.03	...	0.12±0.06	0.15±0.02	0.17	0.16	0.14	0.26	0.21

^aLine ratios are relative to 1-0 S(1) 2.1218 μm .

^bBlack & van Dishoeck (1987).

^cObserved line ratios corrected for effects of telluric lines modeled in Figure 6 and dereddened by $A_K = 2.3, 2.6,$ and 2.1 for Bar1, Bar2, and Orion S.

^d $n_{\text{H}} = 10^6 \text{ cm}^{-3}, \chi = 10^4, T_0 = 500 \text{ K}$ (DB96).

^e $n_{\text{H}} = 10^6 \text{ cm}^{-3}, \chi = 10^5, T_0 = 1000 \text{ K}$ (DB96).

^f $n_{\text{H}} = 10^6 \text{ cm}^{-3}, \chi = 10^5, T_0 = 1500 \text{ K}$ (DB96).

^g $n_{\text{H}} = 10^4 \text{ cm}^{-3}, \chi = 10^2, T_0 = 500 \text{ K}$ (DB96).

^hThermal excitation at $T = 2000 \text{ K}$ (Black & van Dishoeck 1987).

ⁱAn unidentified atomic line near 2.2245 μm has been deblended and subtracted.